Bioelectrochemistry 163 (2025) 108902

Contents lists available at ScienceDirect

Bioelectrochemistry

journal homepage: www.journals.elsevier.com/bioelectrochemistry

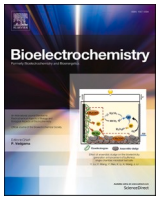

Rapid and receptor-free Prussian blue electrochemical sensor for the detection of pathogenic bacteria in blood

Sriramprabha Ramasamy, Sekar Madhu, Jungil Choi *

Department of Mechanical Engineering, Ajou University, South Korea

ARTICLE INFO

Keywords:
Prussian blue
Bacteria detection
Electrochemical sensor
Bacteria growth monitoring
Blood-based diagnosis

ABSTRACT

Bloodstream bacterial infections, a major health concern due to rising sepsis rates, require prompt, cost-effective diagnostics. Conventional methods, like CO_2-based transduction, face challenges such as volatile metabolites, delayed gas-phase signaling, and the need for additional instruments, whereas electrochemical sensors provide rapid, sensitive, and efficient real-time detection. In this study, we developed a bioreceptor-free Prussian blue (PB) sensor platform for real-time bacterial growth monitoring in blood culture. PB thin films were electrodeposited onto a screen-printed carbon electrode (SPCE) via cyclic voltammetry (CV) technique under optimal conditions. The electrochemical performance of PB/SPCE was assessed using differential pulse voltammetry (DPV) against exoelectrogenic bacteria, including *E. coli*, *P. aeruginosa*, *S. aureus,* and *E. faecalis*. The proposed sensor exhibited surface-controlled electrochemical kinetics and bacteria-driven metal reduction from PB to Prussian white (PW), facilitated by extracellular electron transfer (EET). It showed significant sensitivity with an extensive detection range of 10^2–10^8 CFU/mL for *E. coli* and *S. aureus*, and 10^3–10^8 CFU/mL for *P. aeruginosa* and *E. faecalis*, with reliable detection limits. The sensor accessed the viability of the pathogen within 3 hrs, offering a rapid, efficient alternative to traditional, labor-intensive methods for blood-based diagnostics.

1. Introduction

Sepsis is a severe and often life-threatening condition stemming from bloodstream infections (BSIs) and affects over 20 million people worldwide each year. These infections are caused by the presence of live bacterial and fungal microorganisms in the blood, leading to systemic inflammation and organ dysfunction [1,2]. The occurrence of sepsis caused by bloodstream bacteria varies across different regions and is influenced by factors such as healthcare infrastructure, levels of antimicrobial resistance, and demographics of the population. The most common bacterial pathogens causing BSIs include gram-positive organisms like *Staphylococcus aureus* (SA) and gram-negative organisms like *Escherichia coli* (EC), those frequently associated with healthcare settings, especially in intensive care units (ICUs), where invasive procedures and devices are commonly used [3]. Continued efforts in early detection, effective treatment, and comprehensive data collection are crucial for reducing the worldwide impact of sepsis [4].

Current blood bacteria monitoring techniques include blood culture, nucleic acid-based assays, matrix-assisted laser desorption/ionization time-of-flight mass spectrometry (MALDI-TOF MS), and next-generation sequencing (NGS). These methods help to identify and characterize the bacterial pathogens in the blood, aiding in diagnosis and treatment. However, they have limitations such as slow turnaround times [5], limited sensitivity and false negatives, lack of quantitative data, [6] high costs, and challenges in detecting antibiotic-resistant strains [7]. Tackling these challenges is crucial for improving blood pathogen monitoring and patient outcomes, making persistent research and development essential for advancing clinical diagnostics.

In this context, electrochemical sensors provide a promising alternative, offering a more effective approach for detecting bacterial infections in the bloodstream compared to conventional microbiological techniques. Their rapid detection capabilities [8], high sensitivity and specificity [9–12], portability, cost-effectiveness [13] and potential for detecting antibiotic resistance make electrochemical sensors a valuable tool in clinical diagnostics [14–16]. As technology continues to evolve, electrochemical sensors in medical practice are expected to expand, further improving patient care and outcomes.

Recently, label-free electrochemical sensors have been valued for their ability to monitor pathogens in blood without molecular labels and simplify the process through [17] the electrochemical changes when

* Corresponding author.
E-mail address: cji@ajou.ac.kr (J. Choi).

https://doi.org/10.1016/j.bioelechem.2025.108902
Received 23 October 2024; Received in revised form 26 December 2024; Accepted 5 January 2025
Available online 9 January 2025

bacteria interact with the sensor's surface in real-time [18–20]. Overall, label-free electrochemical sensors provide promising blood pathogen monitoring with potential improvements through advanced materials and expanded research applications in clinical diagnostics and biomedical research [18].

For effective electrochemical monitoring of bacterial growth, kinetic analysis is a valuable tool to reveal the catalytic interactions, particularly electron donors and acceptors in microbial metabolism. Electron transfer between bacteria and the electrode happens through either intracellular electron transfer (IET), or extracellular electron transfer (EET), which involves the use of redox mediators [21]. EET has received significant attention among these methods due to its direct relevance in applications such as microbial fuel cells, corrosion, and sensors. Key components in EET include redox proteins like c-type cytochromes, molecular electron shuttles, conductive pili/nanowires, extracellular polymeric substances, and redox mediators [22].

Many microorganisms derive energy from redox reactions, including aerobic respiration, anaerobic respiration, and the oxidation of reduced inorganic compounds. These processes rely on redox couples such as O_2/H_2O, NO^{3-}/NO^{2-}, and Fe^{3+}/Fe^{2+}. Remarkably, microorganisms can biologically reduce many metals, such as Fe, Mn, Cu, Mo, and Au, providing sufficient energy for their growth. Specifically, Fe^{2+} can act as an electron donor, while Fe^{3+} serves as a terminal electron acceptor in anoxic conditions, supporting the growth of iron-reducing bacteria [23,24].

In this context, PB, a coordination polymer, has gained interest in its use in electrochemical sensing, including the detection of bacteria. Recent advancements have led to the development of PB-based optical, colorimetric, and electrochemical sensors using simple fabrication methods designed for the efficient detection of distinct bacterial strains in wider applications. Vincy *et al.* have developed a robust STAR paper-based colorimetric dipstick sensor that is highly sensitive and utilizes the principle of PB synthesis as a visual indicator [25]. A multifunctional colorimetric nanozyme, AuAg@PB MOF, was synthesized and employed as a dual-mode sensor by J. Cai *et al.* for specific and sensitive bacterial detection [26]. An XGBoost method proposed by Ying Xu *et al.* used a machine learning-based (PB/MWCNT/Au/Anti-BSA-*E. coli*) EIS biosensor to detect the effect of a low-dose inhibitor (e.g., hydrogen peroxide) on *E. coli* [27].

A salient feature of PB as an electron mediator in various sensor designs, facilitating the electron transfer processes that are crucial for the detection of bacterial metabolites or specific bacterial markers [28,29]. For instance, with a high molecular extinction coefficient and suitable redox potential of soluble and insoluble forms of PB-coated ITO-PET electrodes employed in colorimetric and electrochemical metabolic indicators of EC growth monitoring [30]. Likewise, PB has been combined with gold nanoparticles to create a sensitive and specific immunosensor for detecting bacterial canker disease. The versatility of the PB-based sensors designed for the electrochemical detection of EC O157:H7 demonstrated high sensitivity due to the efficient bi-functional role in both recognition and signal amplification in complex biological samples [31]. T.C. Babin *et al.* proposed the non-destructive potentiometric measurement in blood cultures using PB as one of its multi-material electrode arrays and machine learning to identify gram-positive and negative bacterial strains instead of volatile compound CO_2-based transduction methods in blood culture monitoring. Although CO_2 provides generic detection of bacterial growth in blood culture, the phase transfer time between liquid to sensible gas phase is higher in a controlled environment. Also, their findings focused on a polyaniline microarray to detect pH changes for bacterial identification, which necessitates understanding the electrochemical fingerprints (ELFs) of each microorganism [32]. Several aspects remain unexplored, including identifying the redox species involved in the ELFs and monitoring bacterial growth in blood samples.

Building on these insights, we demonstrated the effectiveness of PB for electrochemical bacterial growth monitoring in blood samples, targeting both gram-negative and gram-positive strains. PB was electrodeposited onto SPCE using a simple CV technique under optimal conditions. The sensor's role in bacterial growth monitoring through the EET process was thoroughly investigated and validated using kinetic models and spectroscopic methods. The developed sensor showed high sensitivity, repeatability, and a wide detection range in blood pathogens monitoring. Model bacterial strains growth curves in a mixture of culturing buffer and blood samples were monitored within 3 hrs to measure bacterial viability. The study outcomes emphasized the effectiveness of PB-based sensors for fast bacterial monitoring in blood health diagnostics.

2. Experimental section

2.1. Materials and methods

Hydrochloric acid, potassium iron hexacyanoferrate, iron chloride hexahydrate, potassium chloride, sodium chloride, hemoglobin (human), and bovine serum albumin chemicals were procured from Sigma-Aldrich with analytical grade and used without further purification. The deionized (DI) water with a verified specific resistance of 18 MΩ/cm was employed throughout the experiments. The bacteria culture preparation and electrochemical sensing experiments were carried out using BacT/Alert (FA Plus) buffer −Aerobic (Ref: 410851), sheep blood defibrinated (MB-S1876) from Kisanbio Co. In this work, the bacterial strains collected from standard CLSI strains (American Type Culture Collection) *E. coli* ATCC 25922, *S. aureus* ATCC 29213, *P. aeruginosa* ATCC 27853, and *E. faecalis* ATCC 29212 and used for the electrochemical studies. The volunteers' blood samples were collected from Ajou Health Care Center utilizing the proper safety protocols for real-time blood monitoring studies according to the Institutional Review Board (IRB) guidelines and ethical principles (IRB approval number: 202411-HS-004).

2.2. Preparation of PB/SPCE

The present study explored the electrodeposition of PB on SPCE using the CV technique under optimized experimental conditions. In a typical experiment, 2.5 mM K_3 $[Fe(CN)_6]$ and 2.5 mM $FeCl_3{\cdot}6H_2O$ were dissolved in 0.5 M HCl prepared with DI water. To this solution, 100 mM KCl was gradually added until a homogeneous mixture was obtained. The PB film was then electrodeposited on the carbon electrode within a potential window of −0.4 V to 0.4 V at a scan rate of 50 mV/s. Deposition cycles were varied among 10, 15, and 20 to achieve uniform coating and optimal film thickness for enhanced catalytic properties [33]. Following deposition, the PB-coated samples were rinsed with DI water and dried at 70 °C for 24 hrs, and kept in a desiccator before use.

The CV profiles showed an increase in redox peak currents in successive cycles during electrodeposition, indicating PB nucleation, which stabilized as a uniform thin film after 20 cycles. Surface analysis revealed that increasing the number of deposition cycles resulted in thicker films (C10: 3.45 μm, C15: 6.13 μm, C20: 9.94 μm) and greater surface roughness (Bare SPCE: 1.890 μm, C10: 2.16 μm, C15: 2.29 μm, C20: 2.52 μm). This increase in surface roughness is expected to contribute significantly to the enhanced catalytic behavior of PB in biosensor applications. Detailed optimization including cycling profiles, 3D laser surface analysis, and preliminary electrochemical results are provided in the supplementary information (Fig. S1-S2).

2.3. Material characterization

The morphological features and elemental information of the developed materials were determined using field emission scanning electron microscopy (FESEM, JEOL-JSM-7900F, Japan) with an accelerating voltage of 10 kV and an energy dispersive X-ray spectroscopy (EDS). X-ray diffraction (XRD, Rigaku Ultima IV, Japan), Fourier

transform infrared (FT-IR) spectroscopy (Nicolet iS50, Thermo Scientific), Raman spectroscopy (Renishaw InVia Raman microscope, with an excitation laser of 514 nm), and X-ray photoelectron spectroscopy (XPS, Multilab 2000, UK) were employed to examine the crystal structure, functional groups, chemical composition, and surface chemistry of PB/SPCEs, which is essential in terms of their electrochemical sensor ability. AutoCAD 2024 software was used to design custom-sized SPCEs with a three-electrode system. SPCEs were fabricated using a semi-automatic screen-printing instrument using commercial conductive inks, including a graphite working electrode (WE), a Pt counter electrode (CE), and an Ag/AgCl reference electrode (RE). The electrochemical analyses were conducted by utilizing an electrochemical workstation (PalmSens 4, Netherlands). The surface coverage, film thickness and roughness of prepared PB/SPCE samples were evaluated using 3D-Laser profiler, (Maker: KEYENCE and Model: VK-X250K/X260K). The concentration of bacterial strains was adjusted using a DensiCHEK Plus densimeter for electrochemical sensitivity analysis.

2.4. Bacterial culture conditions

The bacterial stock cultures of interest in the present study were revived and streaked on Luria broth (LB) agar plates and incubated overnight at 37°C. The grown colonies of each bacterial strain from the agar plate were picked and inoculated in 1 mL of BacT/Alert buffer separately. An aliquot of 4 mL bacterial cultures with sheep and human blood was diluted, and their concentration was adjusted using a densimeter from 10^2 to 10^8 CFU/mL.

3. Results and discussion

3.1. Morphological, structural and chemical composition analysis

The FESEM image shown in Fig. 2a illustrates the sheet-like morphology of the graphitic carbon ink (as clearly emphasized in the inset) used for fabricating the working electrode (WE) on the SPCE. Fig. 2(b and c), imply the cubical morphology of the prepared PB nanostructures, with an average edge length of ~ 66 nm. The nanocubes are uniformly grown throughout the surface of the carbon electrode. Further, the EDS spectrum in Fig. 2d and color mapping from Fig. 2(e-i) confirm the phase purity, elemental composition, and uniform distribution of PB over the substrate. The PB nanocubes, with notable active surfaces, could improve their catalytic behavior and preferable charge transfer ability between the PB and cell wall of the bacterial strains with surface adhesion during the electrochemical reaction.

Fig. 3a displays the XRD patterns of the bare and electrodeposited PB/SPCEs. The crystalline peaks of the bare electrode at 18°, 22.6°, 28°, 31°, and 58° indicated the presence of the graphite ink used to design the WE [34]. The strong and sharp diffraction peaks of PB/SPCE, counting (200), (220) (400), (420), (440), (600), (620), (640), and (642) confirmed the face-centered cubic (FCC) PB lattice in which, Fe(III) ions connected to Fe(II) and nitrogen atoms in the 3D skeleton surrounded by carbon atoms of cyanide ligands. The outcomes were closely examined and validated against the standard diffraction pattern of PB (Card No: 00-073-0687) and the crystallite size was determined to be ~ 4 nm using conventional Scherrer's formula. Additionally, a subtle shift towards a higher angle was seen in a few diffraction peaks namely (440), (600), and (620) and this might be attributed to the presence of structure distortion in the FCC structure, which would have a considerable influence on the catalytic behavior of the material in sensor applications [35,36].

The wide-angle XPS spectra were used to examine the chemical compositions and different oxidation states of elements of bare and PB/SPCE as shown in Fig. 3b. As anticipated, survey spectra of bare SPCE showed the photoelectron lines for C, and O associated with the graphite ink. Further, the PB deposited SPCE confirmed the presence of Fe, C, N, and O elements, ensuring its primary constituents.

The peaks observed at 281.9 eV correspond to the C1s band, while the O1s peak is detected at 530.3 eV. The broad and less intense peak at 976.3 eV represents the O KLL transition, which arises from the ejection of electrons due to the filling of the O 1s state (K shell), coupled with the

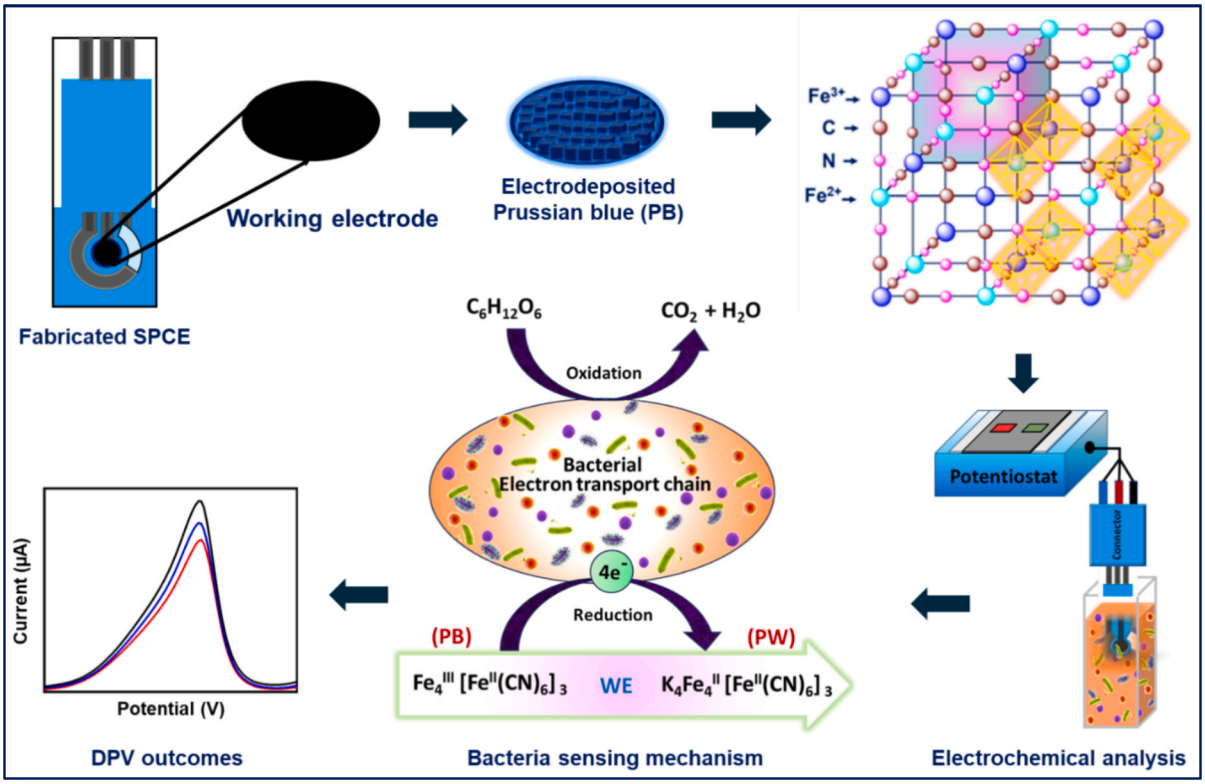

Fig. 1. Schematic illustration of the fabrication and electrochemical bacterial detection of PB/SPCE.

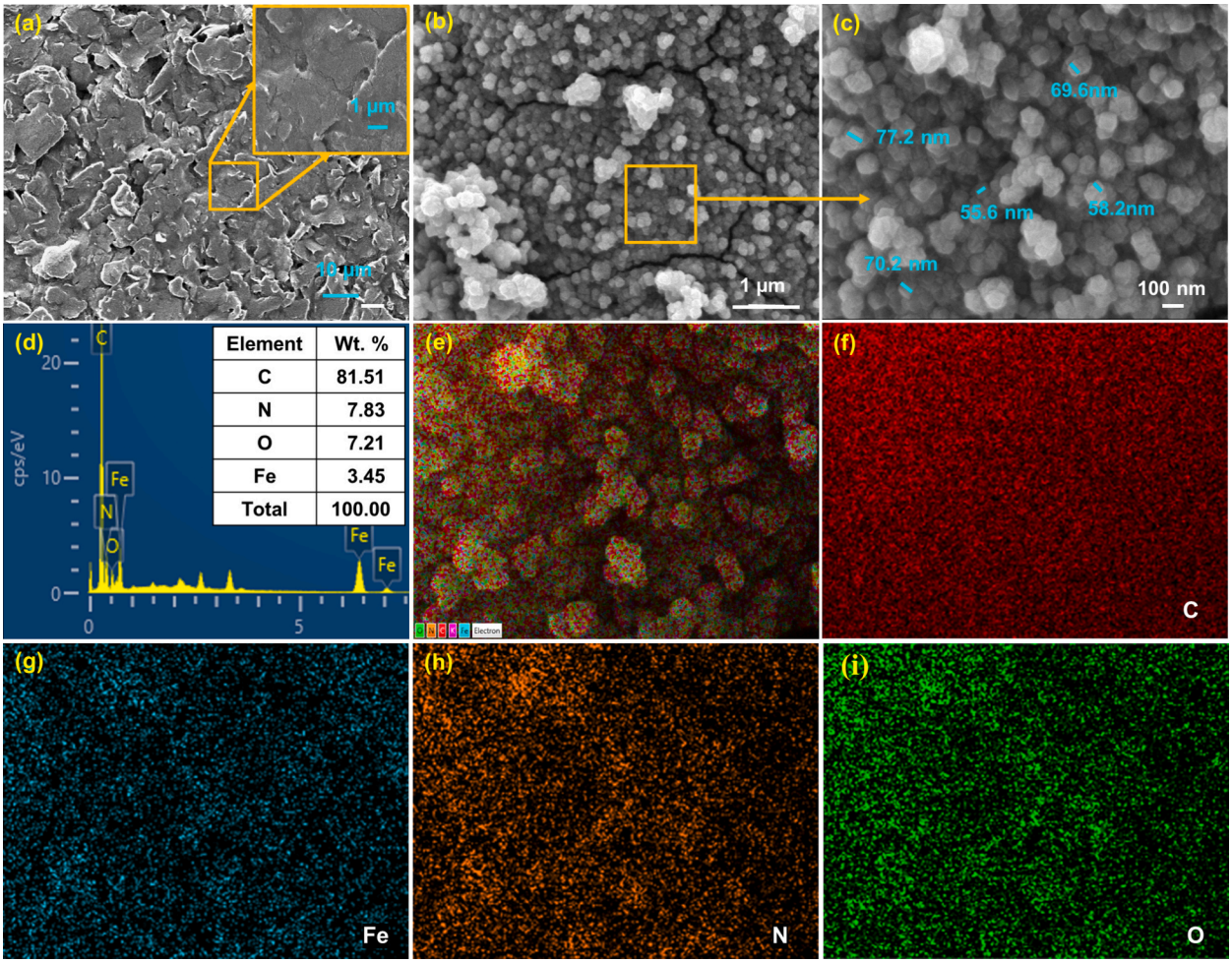

Fig. 2. FESEM images of (a) bare SPCE, (b and c) PB/SPCE, (d) EDS spectrum and color mapping analysis of (e) collective element distribution, (f) carbon, (g) iron, (h) nitrogen and (i) oxygen of PB/SPCE.

simultaneous ejection of an electron from an L shell. The C 1s spectrum of PB/SPCE resulting from M'-C≡N-M structure, and binding energy of 395.9 eV consistent with the metal-nitride bonding. The presence of Fe $2P_{1/2}$ was identified with the photoelectron line at 708.0 eV and Fe $2p_{3/2}$ was found at 713.4 eV. Thus, the survey spectra confirm the successful formation of PB nanostructures on the working electrode [37], and changes in oxidation states of PB/SPCE constituents before and after bacteria sensing will be discussed in detail with their respective deconvolution spectra in the electrochemical analysis section.

The existence of functional groups in PB/SPCE has been confirmed using the FT-IR spectrum as shown in Fig. 3c. A broad peak at 3631 cm^{-1} associated with OH stretching vibration of the surface absorbed water and hydroxyl group of PB [38]. The Fe(II)–CN-Fe(III) network could be identified in the mid-range of FT-IR spectra, between 2400 and 1800 cm^{-1}. The foundation of an intense and sharp band at 2082 cm^{-1} is attributed to Fe(II), and its accompanying weaker band at 2323 cm^{-1} is consistent with Fe(III) identifies the ν(CN) stretching vibration band of Fe(II)−CN–Fe(III) skeleton of FCC PB structure. The peak at 1722 cm^{-1} ensures C═O stretching mode and C-OH vibration aroused in the range of 1487–1434 cm^{-1}. The characteristic vibrational modes of the cyano-complex, such as ν(NCO) and ν(Fe–C), are located between 1287–1074 and 635 cm^{-1}, respectively. In the lower range of FT-IR spectra, the peak at 965 cm^{-1} corresponds to the symmetric and asymmetric stretching of the $_{\nu}$(C≡N), vibration band. The cyano-complexes exhibited ν(Fe–C), and δ(Fe–CN) bands, which are located at 605 and 501 cm^{-1} [39].

Raman spectra offer detailed yet complex insights into the chemical composition and information of molecular vibrations of prepared materials. In the Raman spectra, the bare SPCE showed signature vibration modes including the G band (1587 cm^{-1}) and D band (1350 cm^{-1}) originating from graphite ink. The Raman spectrum of PB/SPCE reveals the specific vibrational modes of its crystal lattice including the C≡N group, coordinated with Fe ions of various valence states. The primary peak, around 2086 to 2157 cm^{-1}, corresponds to the $1A_g$ ν(CN) stretching vibration and the [Fe(II), Fe(III)] vibrational states. Additional peaks appeared in the lower energy region, between 185–368 cm^{-1} corresponding to the Fe–CN–Fe bond, while a shoulder peak at 181 cm^{-1} is related to C–Fe–C deformation vibrations. The well-intense peak (534 cm^{-1}) observed in the range of 409–672 cm^{-1} is associated with Fe–C stretching vibrations. The spectra can differentiate between various iron oxidation states (Fe(II) and Fe(III)) within PB by detecting shifts in the vibrational peaks, which helps in understanding the redox chemistry of PB [40,41].

3.2. Electrochemical analysis

3.2.1. CV and DPV analysis of PB/SPCE in bacteria growth buffer and sheep blood

Electrochemical methods have been employed to investigate bacterial metabolites due to their intricate internal and external electron transport mechanisms. In this work, we explored the electrochemical properties of PB-coated SPCE to monitor the growth of two gram-positive and gram-negative bacterial strains. Initially, CV experiments were conducted using a mixture of 3 mL BacT/Alert (FA Plus) buffer and 1 mL of defibrinated sheep blood, in the absence of bacteria with an

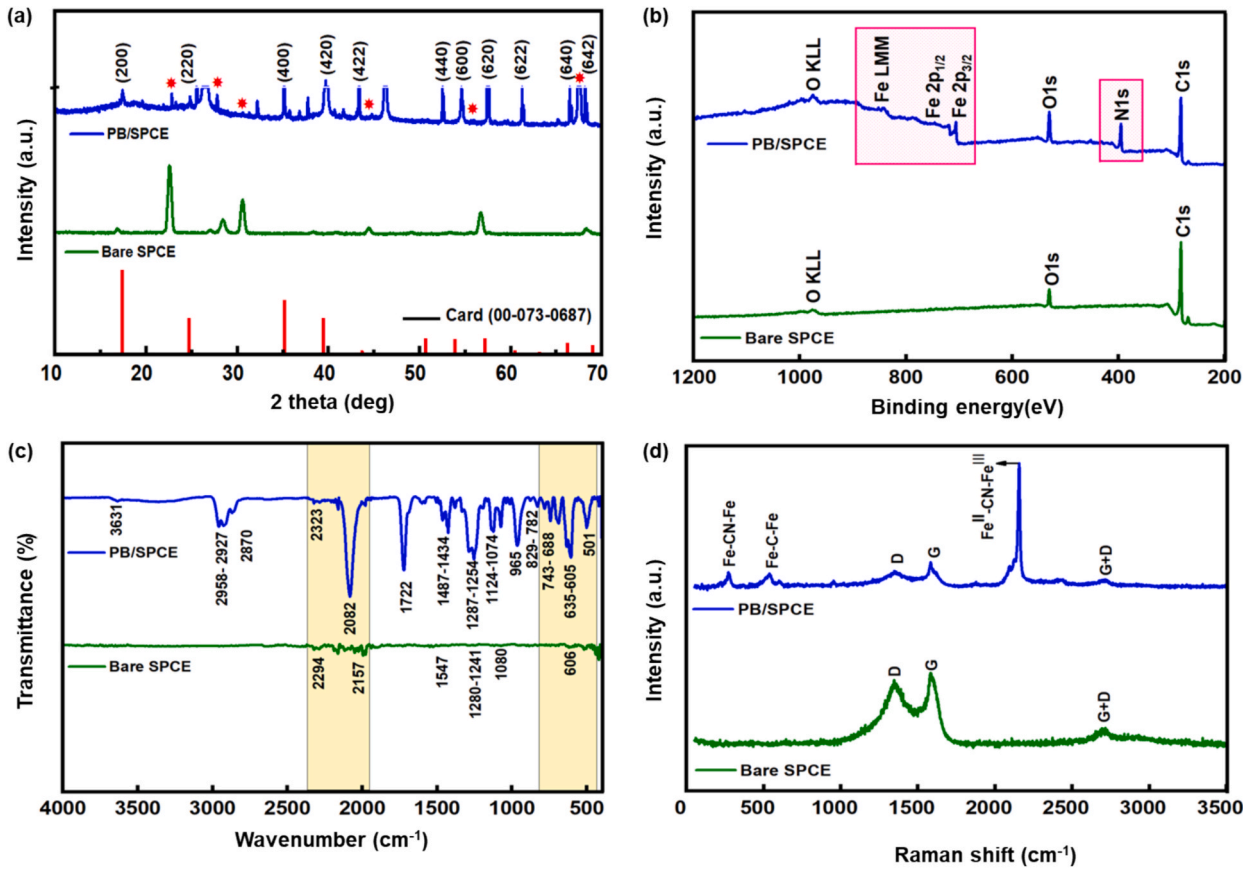

Fig. 3. (a) XRD, (b) XPS survey spectra (c) FT-IR, and (d) Raman spectra of bare and PB/SPCE.

optimal potential window of −0.5 V to + 0.5 V and 50 mV/s scan rate.

The PB/SPCE displayed a well-defined redox pair in the BacT/Alert buffer in between −0.05 V and 0.05 V with peak current of ± 130 μA, while the bare SPCE showed no discernible redox in the electrolyte (Fig. 4a). In the context of the sheep blood and buffer mixture, complex molecules caused a minor shift in potential in the redox response, along with a slight decrease in peak current compared to the buffer alone.

Fig. 4b illustrates the redox peak current response of PB/SPCE from the DPV analysis, showing a reduction peak at −0.05 V in the bacterial growth buffer, which shifts to 0.15 V in the presence of the sheep blood mixture buffer. Further, the smaller decrement in peak current might be due to the complexity of blood composition. PB is known for its excellent ion exchange characteristics, which enable it to bind to specific metal ions and form stable complexes. Further, the cyclic and long-term stability along with the effect of pH of prepared PB/SPCE sensors were verified and the outcomes are provided in Fig. S3-S5. Moreover, the EIS analysis was examined in the frequency range of 40 Hz to 200 kHz based on the interfacial impedance at the electrode surface to assess the charge transfer properties of the prepared PB/SPCE in the presence and absence of model bacterial strains within bacterial culture buffer and blood mixtures and the details given in Fig. S6 [42,43].

3.2.2. Scan rate analysis

The electrochemical kinetics of PB/SPCE were evaluated by observing redox responses at various scan rates (10–100 mV/s) over a potential range of − 0.5 V to + 0.5 V. As the scan rate increases, PB/SPCE demonstrated a notable increase in current with a slight potential shift between cycles, as shown in Fig. 4c. This analysis helped to identify the redox molecules, such as oxygen in the buffer and blood components, that diffuse to/or from the electrode surface, reflecting their bioavailability in the sample. Fig. 4d displayed the linear plot of log (scan rate) *vs.* log (peak current) indicating that the electrochemical reaction was a surface-controlled process [44] and the corresponding linear regression equation is given as follows,

$$I_{pa} = 0.9362x + 0.337\left(\frac{mV}{s}\right) R^2 = 0.9723 \quad (1)$$

$$I_{pc} = 0.9319x + 0.395(mV/s) R^2 = 0.9946 \quad (2)$$

3.2.3. CV analysis of PB/SPCE in the presence of exoelectrogenic model bacterial strains

In this investigation, electrochemical monitoring was performed on exoelectrogenic bacterial strains utilizing PB/SPCE, which included the gram-negative strains EC and PA, as well as the gram-positive strains SA and EF. The bacterial strains were grown in LB media and further diluted to concentrations ranging from 10^2 to 10^8 CFU/mL for subsequent CV and DPV analyses. In the CV study (Fig. 5a), the PB/SPCE demonstrated a substantial redox reaction in the bacterial growth buffer while spiking of EC strains (10^4 CFU/mL) resulted in a significant drop in current as shown in inset (6.25 μA). The result confirmed the reduction of PB/SPCE due to the EET process, attributed to the metal reduction affinity of the EC cell membrane through its metabolic activity. PB is identified as a potential mediator in bacterial growth buffers and blood through the reduction of PB into PW is used to indirectly quantify the concentration of H_2O_2 associated with bacterial strain metabolic activity [45]. According to the findings of Xiao *et al.,* surface-modified GCE with drop-cast EC demonstrated clear electrochemical redox fingerprints at defined potential ranges: − 0.4 V (group I), − 0.2 V to 0 V (group II), and 0 V to 0.4 V (group III). The redox peak at − 0.4 V can be ascribed to flavins that are excreted from EC during growth and peaks in − 0.2 to 0.4 V (groups II and III). They also noted that regions II and III often overlapped in most buffers due to their complexity, both contributing to the gradient in the current response [31].

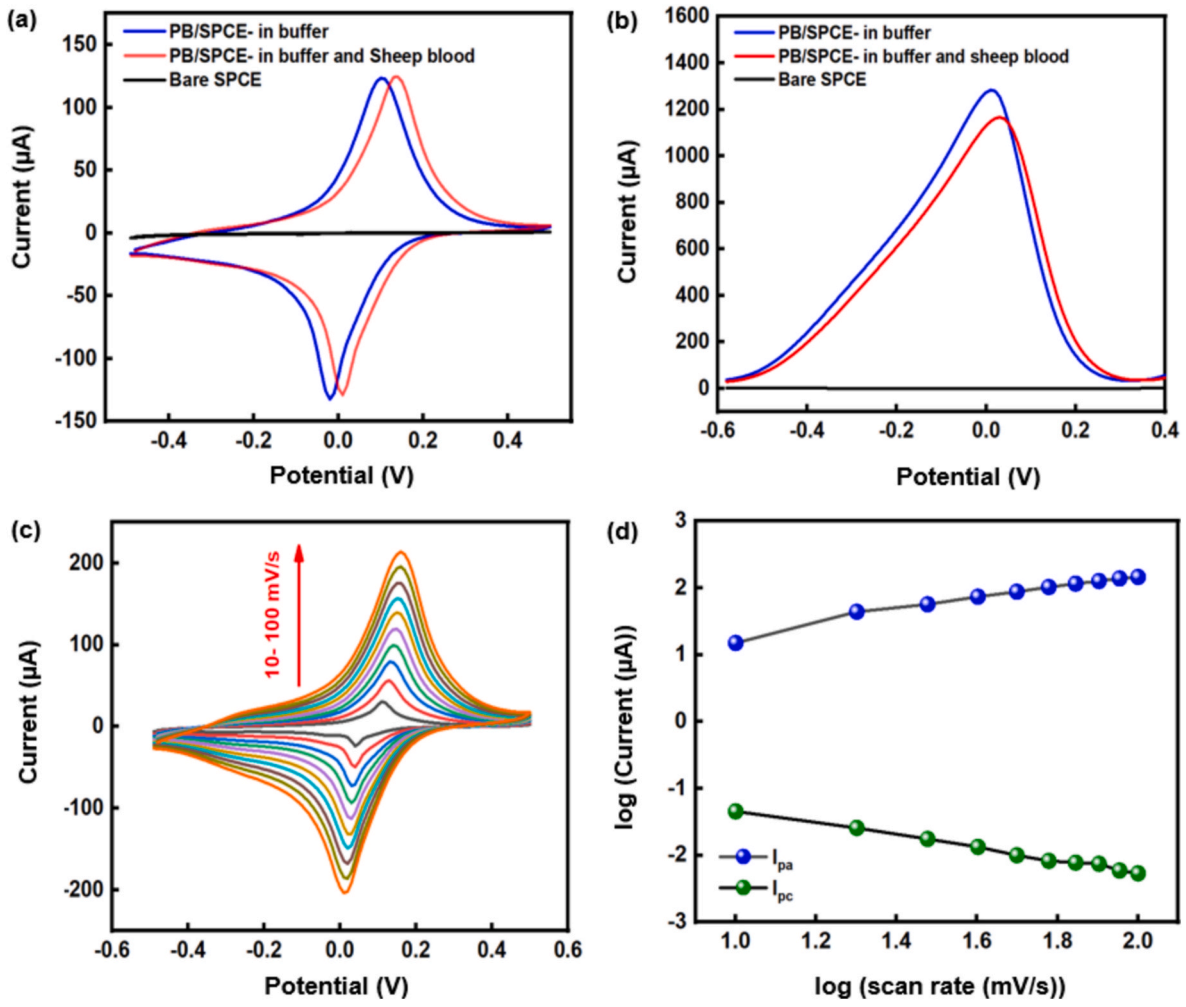

Fig. 4. (a) CV and (b) DPV analysis of bare and PB/SPCE, (c) scan rate analysis of PB/SPCE in the mixture of BacT/Alert buffer and sheep blood (4 mL) in the absence of bacterial strains and (d) corresponding linear plot between log (scan rate) *vs.* log (peak current).

In this analysis, a redox peak was identified in the overlapping region of groups II and III, where a slight decrease in current was observed in the presence of EC strains undergoing the EET process from their cell membranes. In this, charge transfer reaction, possible glucose in culture serves as the electron donor and Fe(III)/Fe(II) as the electron acceptor, and the proposed bacterial sensing mechanism is illustrated in Fig. 1. This electrochemical behavior was supported by Raman analysis, which demonstrated considerable changes in the Fe(III)/Fe(II) vibration modes of PB on SPCE during electrochemical experiments, both in presence and absence of EC strains in the buffer (Fig. 5a). As shown in the Raman spectra in Fig. 5b, the intensity of the characteristic peaks at 2150 cm^{-1}, corresponding to Fe(II)–CN-Fe(III) and the Fe-CN-Fe skeleton of the coordination polymer were decreased.

This reduction is attributed to the transformation of PB into PW and the potential adsorption of pathogens (EC) on the electrode surface. In the presence of PA, PB/SPCE exhibited a similar decrease in redox current of 4.33 µA (Fig. 5c with inset), attributed to extracellular electron shuttles (redox mediators) that facilitate the electron transfer from the bacteria to the electrode surface, as confirmed in Fig. 5d. For the gram-positive exoelectrogenic bacterial strains SA and EF, the PB/SPCE showed a reduction in current 5.72 µA and 4.62 µA along with a slight potential shift, as seen in the magnified image of Fig. 5(e and g inset). The metal-reducing activity (Fe(III)/Fe(II)) was also validated for these strains, with the results presented in Fig. 5 (f and h). These redox potential changes were caused by stress in the bacterial cultures, especially in gram-positive strains, which lack glutathione (GSH) to regulate and maintain redox balance [46]. In the current study, we confirmed that the proposed model bacterial strains exhibited significant electrochemical responses in a mixture of BacT/Alert culture buffer and blood. The sensitivity and growth monitoring of these bacterial strains were further analyzed using the sensitive DPV technique [23].

3.2.4. *Sensitivity analysis*

Electrochemical sensitivity analysis of the proposed PB/SPCE was conducted for all four model pathogens using the sensitive DPV method. Initially, PB/SPCE was examined in BacT/Alert growth buffer with non-infected sheep blood. Serially diluted bacterial strains (EC, SA, PA, and EF) were spiked into blood culture buffer from 10^2 to 10^8 CFU/mL, and their corresponding DPV signals were recorded at an optimal time interval of 15 min. The results shown in Fig. 6(a-h) are consistent with CV outcomes. A linear decrease in peak current as bacterial concentration increased is evident from the metal-reducing abilities of the tested bacterial strains.

The differences in detection thresholds among the pathogens indicate that the electrochemical behavior of each species contributes to the variations in the observed current. A linear relationship between the concentration and peak current values confirms the sensitivity of PB/SPCE (slope value, Fig. 6) with the detection ranges of 10^2–10^8 CFU/mL for EC and SA, and 10^3–10^8 CFU/mL for PA and EF. Further, the lower detection limit (LOD) of PB/SPCEs towards the model bacterial strains was calculated as 1.01×10^2 CFU/mL for EC, 0.6×10^2 CFU/mL for SA and 3.97×10^3 CFU/mL for PA and 1.55×10^3 CFU/mL EF respectively

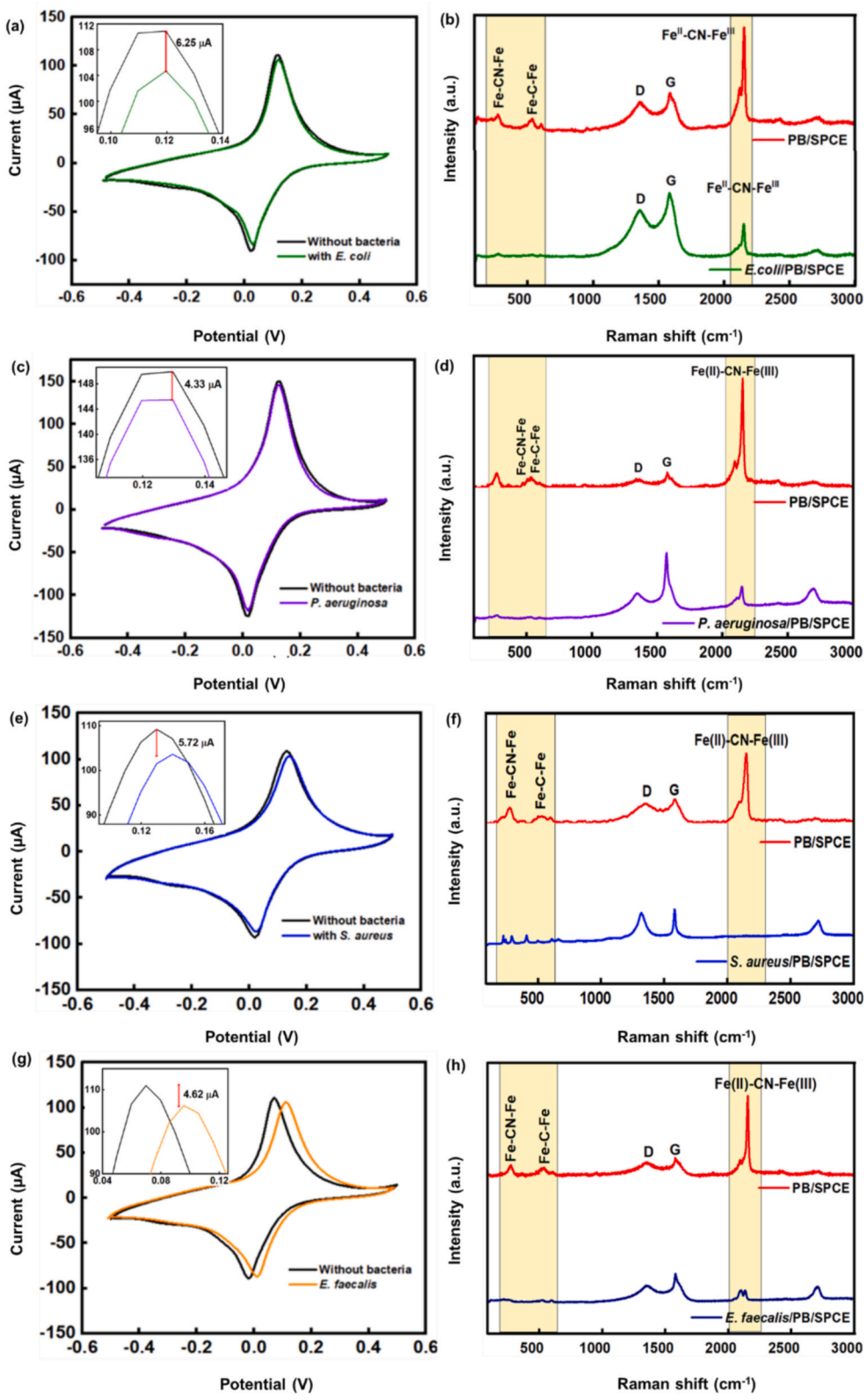

Fig. 5. CV analysis of PB/SPCE in 4 mL mixture of BacT/Alert buffer and sheep blood in the absence and presence of (a) EC (c) PA, (e) SA, (g) EF bacterial strains (10^4 CFU/mL) and (b, d, f and h) their respective Raman spectra.

and details are given in the supplementary information (Table S2). These experiments demonstrated the utility of the PB/SPCE for pathogen detection and highlighted the method's sensitivity for different bacteria in a complex medium.

XPS analysis is highly effective for examining microbial surface composition, offering precise and quantitative data on chemical bonds and elements on microbial cell surfaces. In this study, the electrochemical interaction between EC bacterial strains and the PB electrode surface was investigated, and the results are depicted in Fig. 7. Specifically, the analysis focused on the C 1s binding energy peak on bacterial

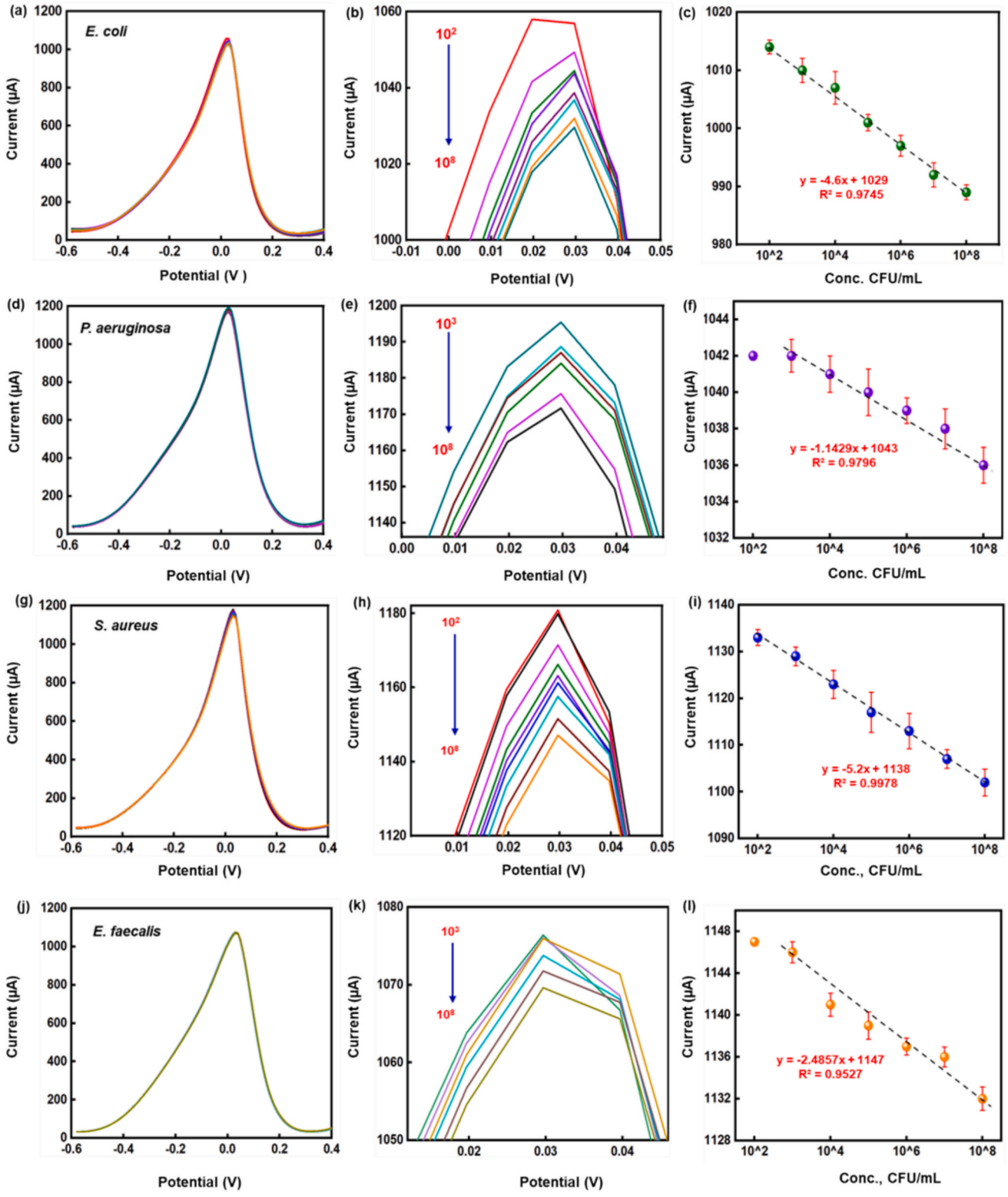

Fig. 6. DPV analysis of PB/SPCE in 4 mL mixture of BacT/Alert buffer and sheep blood with targeted bacterial strains (a) EC, (d) PA, (g) SA, (j) EF at different concentrations, (b, e, h and k) their magnified images and (c, f, i, and l) linear plot between concentration *vs.* peak current.

cell surfaces, which includes four carbon-based components with varying binding energies. Notably, the reduction of PB into PW during the metabolic activity of the bacterial growth could be confirmed from the possible changes in the iron redox states Fe(III)/Fe(II) on the PB/SPCE surface. Therefore, we evaluated the PB/SPCE in the buffer before and after the addition of EC strains, and their survey spectra are illustrated in Fig. S7, in which no significant variations were found in the surface components of PB/SPCE when examined in BacT/Alert buffer and sheep blood in the absence of bacteria.

However, in the deconvolution spectra of PB/SPCE before and after sensing EC bacteria (Fig. 7(a-h)), noticeable changes were observed in the C 1s, N 1s, and Fe 2p photoelectron spectra due to the interaction of

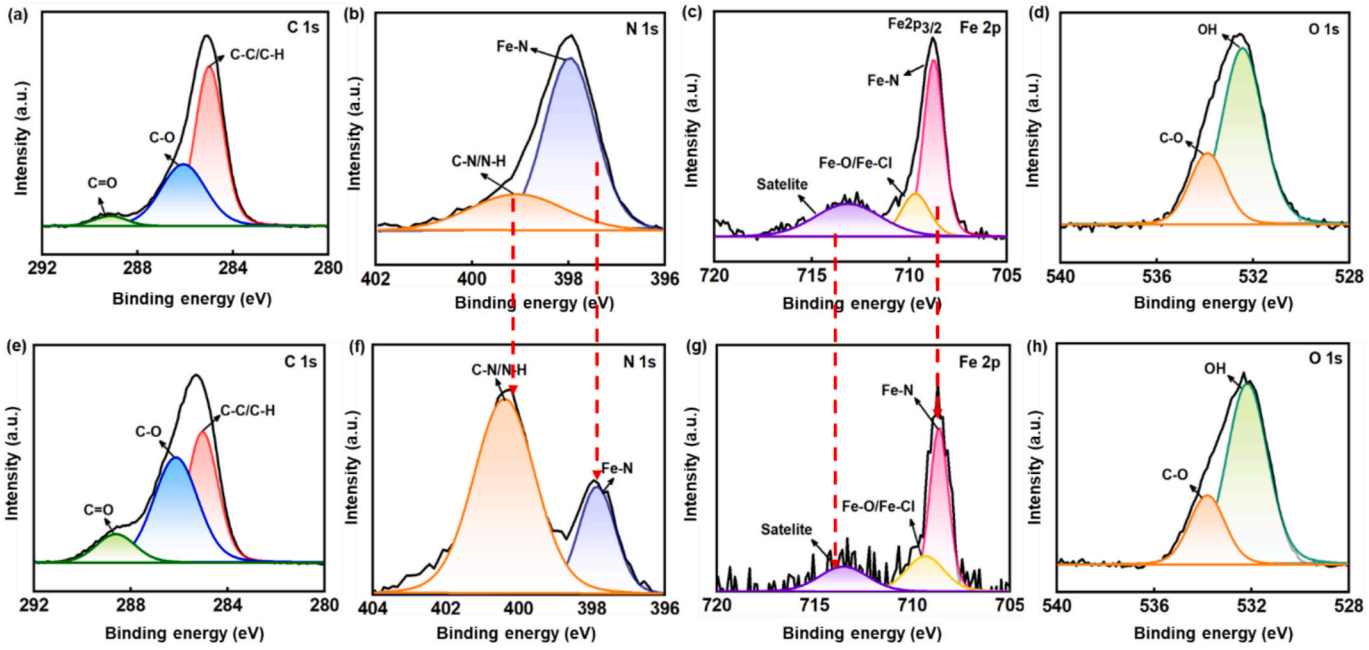

Fig. 7. XPS deconvolution spectra of PB/SPCE (a-d) before and (e-h) after electrochemical sensing of bacteria in a mixture of BacT/Alert buffer and sheep blood.

the bacterial surface components with PB [47]. The C 1s spectrum of PB/SPCE following bacteria sensing showed a significant increase in photoelectron intensities linked to C=O at 286.2 eV and O=C-OH functionalities at 288.6 eV, attributed to the higher oxygen content on the bacterial cell surface (Fig. 7e). The peak corresponding to Fe^{3+} ions have low spin found in the range of 710.5–713.0 eV bound to cyanide ligands, creating a rigid, ordered structure with strong Fe-C≡N-Fe bonding whereas Fe^{2+} have high-spin, observed in 708.5–709.0 eV coordinated to nitrogen atoms.

The Fe 2p spectra given in Fig. 7c showed an apparent decrease in the satellite peak at 713.4 eV after the bacteria interaction (Fig. 7g) confirmed the reduction of Fe(III) to Fe(II) due to the EET process from the bacterial cell membrane. This could be further validated from N 1 s spectra (Fig. 7f), the intensity of the Fe-N photoelectron line at 397.8 eV decreased due to the changes in cyanide coordination. Moreover, the area corresponding to C-N/N–H binding energy at 400.3 eV, associated with the PB coordination polymer, increased due to the adsorption of bacterial cell proteins containing amide functionalities during the bacterial growth phase. These XPS findings suggest valuable insights into the metal Fe(III) reducing activity of exoelectrogenic EC bacterial cell surfaces.

3.2.5. *Bacterial growth monitoring in sheep blood*

To assess the viability of the proposed electrochemical sensor for identifying bloodstream infections, four bacterial strains (10^2 CFU/mL) were introduced into a bacterial growth buffer mixed with whole blood. The DPV current response of PB/SPCE was recorded at 1 hr intervals over a 13 hrs time-lapse study for all four model pathogens in positive sheep blood culture samples, reflecting growth in response to PB/SPCE metabolic reductions. Fig. 8 illustrates the correlation between time (hrs) *vs.* peak current and colony count (CFU/mL), along with plate counting details and the results indicated a gradual reduction in peak current, confirming an increase in bacterial population, which was further validated through plate counts over time. We employed the standard plate count method to estimate the bacterial population density in a sample by plating a small, diluted portion and counting the resulting bacterial colonies. Among the selected model bacterial strains, EC, SA, and EF were observed to have a doubling time of 20 min, whereas PA exhibited a slower growth rate with a doubling time of 3–6 hrs. Consequently, blood culture plating was performed at 3 hrs intervals over the 12 hrs electrochemical analysis. The number of colonies observed was correlated with the current differences obtained from the DPV profiles of each bacterial strain over time, as shown in Fig. 8.

Notably, EC and SA displayed a higher growth rate, resulting in greater current differences during the 12-hour analysis. In contrast, the growth profile and DPV current differences of EF strains appeared moderate, while the slower growth rate of PA resulted in smaller current differences over the same period. The observed colony counts during bacterial growth monitoring were consistent with the estimated empirical values and a positive correlation was observed between the plate count and current signals from the sensor confirming the reliability of the sensor for practical applications.

These experiments were repeated several times to ensure a consistent bacterial growth profile under the selected experimental conditions. The DPV analysis of PB/SPCE demonstrated in Fig. S8 (a and b) indicates that there has been no discernible decrease in the current responses in the absence of bacteria in the buffer mixtures, including sheep and human blood. Additionally, the increment in current responses is attributed to the catalytic properties of PB, which facilitate the electrooxidation of blood components, including proteins and amino acids [32,48,49]. Further, we evaluated the performance of PB/SPCE in the presence of potential blood-borne interfering compounds, including ions such as K^+ (5 μM), Na^+ (150 μM), Fe^+ (0.5 mg), and proteins such as BSA (1.6 mg/mL) and hemoglobin (Hb, 200 mg/mL), at their maximum reliable concentrations in blood. The corresponding DPV results are presented in Fig. S9. The results ensured the reliable performance of PB sensors in pathogen monitoring in blood.

The bar diagram of the control study with non-infected blood (no bacteria present) and various initial concentrations (10^1 and 10^2 CFU/mL) of model bacterial strains is shown in Fig. S10. The time-lapse analysis revealed similar patterns of current reduction for both initial concentrations during bacterial growth. However, the peak current differences were slightly higher at 10^2 CFU/mL compared to 10^1 CFU/mL after 12 hrs of observation. Moreover, PA bacteria take more time to grow, and the change in their peak current over time is less pronounced compared to other models of bacterial pathogens. Further, the viability of the proposed pathogens in the presence of PB nanoparticles was verified using bacterial growth in culture plates as given in Fig. S11. The

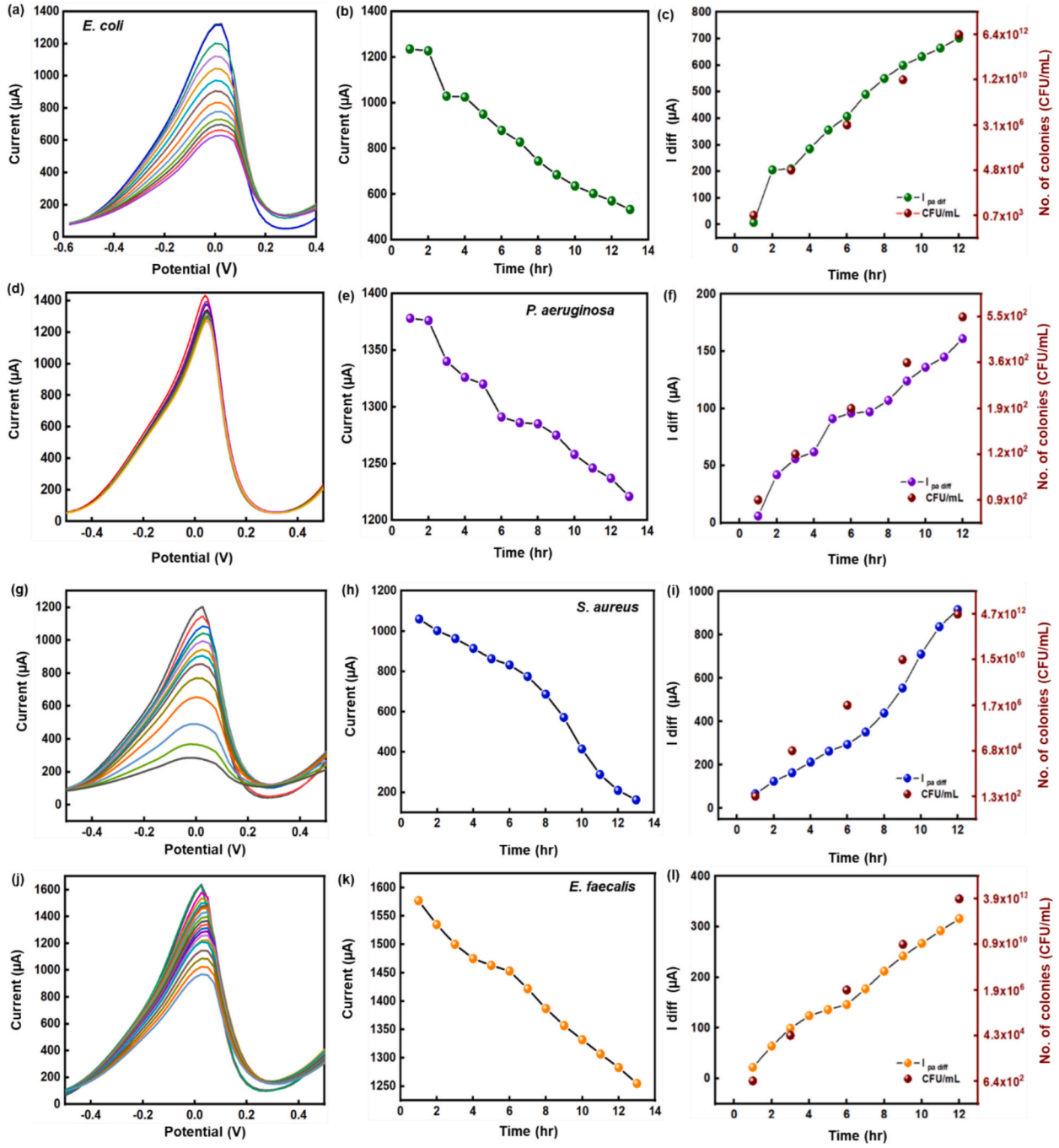

Fig. 8. DPV time-lapse analysis of PB/SPCE in a mixture of BacT/Alert buffer and sheep blood (4 mL) in the presence of target bacterial strains (a) EC (d) PA, (g) SA, (j) EF (with initial concentration10^2 CFU/mL), (b, e, h and k) linear plot between peak current and (c, f, i and l) linear plot of time *vs.* peak current difference and no. of colonies (CFU/mL).

redox profile of PB/SPCE was influenced by the complexity of the buffer and blood components. The metal-reducing ability of these exoelectrogenic bacterial strains, stemming from electrostatic and metabolic interactions, validated their viability.

3.2.6. Bacterial growth monitoring in the human blood in real-time

The reliability of the PB/SPCE sensor in monitoring bacterial growth in human blood samples was collected from volunteers using the identical DPV experimental conditions as in the time-lapse analysis. The DPV results from human blood-positive cultures in the presence of model pathogens showed similar trends in current decrement. However, the differences in current magnitude observed in Fig. 9(a-l), are likely due to variations in the concentration of blood cells and viscosity between sheep and human blood which affects the rate of metal-reduction ability of the bacterial strains. From the linear plot, a log phase of bacterial growth was observed for up to 7 hrs, after which the growth shifted toward the stationary phase for around 8 hrs. The apparent growth pattern of these model pathogens is evident from the log phase within 3 hrs as shown in Fig. 9(c, f, i, and l).

Traditional CO_2-based label-free systems require at least 12 hrs of monitoring to validate bacterial growth. This is because a greater bacterial population is required for achieving detectable changes in CO_2 levels as its higher phase transitions time delay in the buffer [32]. However, our study outcomes ensure the competence of the proposed

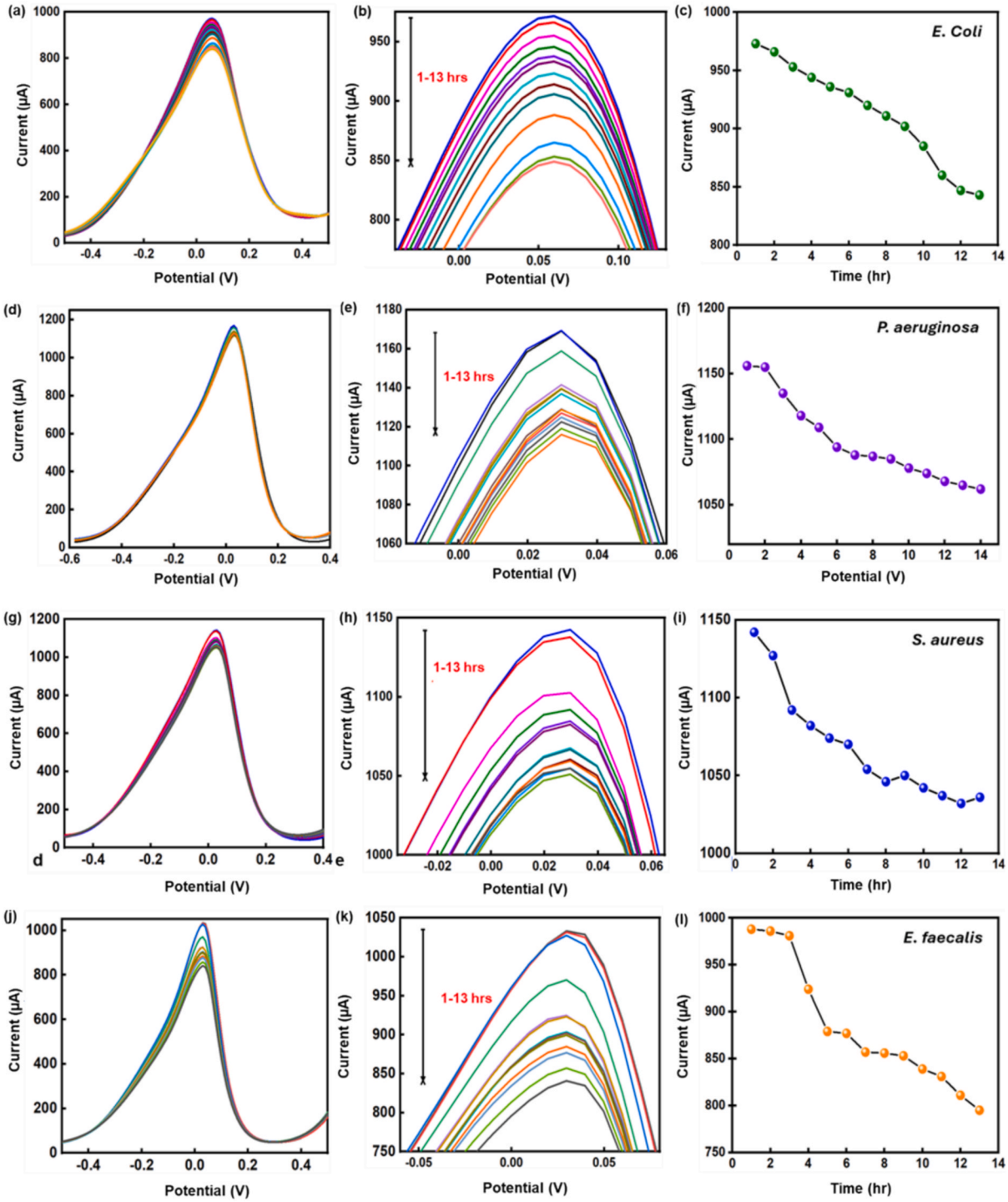

Fig. 9. DPV time-lapse analysis of PB/SPCE in a mixture of BacT/Alert buffer and human blood (4 mL) in the presence of (a) EC (d) PA, (g) SA, (j) EF bacterial strains (with initial concentration10^2 CFU/mL), (b, e, h and k) magnified image and (c, f, i and l) linear plot between time *vs.* peak current.

sensor to monitor bacterial growth within 3 hrs, offering a faster alternative to traditional clinical methods.

Further, a few earlier reports on electrochemical bacterial growth monitoring in blood samples using label-based and label-free approaches are evaluated with the proposed sensor listed in Table 1. Additionally, the effectiveness of PB in detecting bacteria in various body fluids and transduction methods, as demonstrated in earlier literature, is summarized in Table S3. The outcomes ensured that enhancing the redox chemistry of PB could accelerate the EET process and improve its catalytic interaction with different bacterial strains. Moreover, the study suggested that rapid bacterial detection and species identification can be further enhanced by adjusting the functional properties of PB and its analogues.

4. Conclusion

This work described the efficiency of electrodeposited PB nanostructures towards bacterial growth monitoring in blood culture. The electrochemical sensing performance of PB-modified electrodes was evaluated using CV and DPV techniques involving two gram-positive

Table 1
Comparison table of previously reported bacteria sensing works in blood samples.

Working Electrode	Electrode preparation	Target Bacteria	Probe	Detection method	Linear range (CFU/mL)	LOD (CFU/mL)	Ref.
Probe RNA/capture probe RNA//MCH/HDT/Au/Plastic	Sputtering	EC, PA, PM and SA	rRNA	CA	10^4–10^8	10^4	[50]
Probe Casin blocker/capture probe RNA/MCH/HDT/Au/Plastic	Sputtering	EC	16S-rRNA	CA	10^4–10^8	–	[51]
Ab Biotin/BSA/Avidin/EDC/NHS/DTNB/MOF/Au NPs/SPCE	Solvo thermal, electro deposition	EC EC K12	Antibody	CV	10^1–10^7	10^1	[52]
ss-DNA/AuNPs MPTS/SPE	Wet chemical	*S. typhi*	Bacteriophage	CV	2–10 μg/mL	1.91 μg/mL	[53]
PEI-f-CNT	Electro deposition	MRSA, PP and EC	Bacteriophage	EIS	10^1–10^8	1.29 x 10^2	[54]
MB-DNAzyme/Nano Au-FS/Polystyrene	Sputtering, CVD and electroplating	EC and SA	DNA	DPV	10^2–10^5	10^2	[55]
Sal-CAF-GQDs-AuNPs/GCE	Thermal pyrolysis, dropcating	*S. typhi*	Label free	CV	10^3–10^5	32.6	[56]
Au/Cys/GluSS DNA probe//DNA *S. typhi*	Wet chemical	*S. typhi*	DNA	DPV	0–10 μg/mL	1.91 μg/mL	[57]
PB/SPCE	CV-electro	EC, SA	Label free	DPV	10^2–10^8	1.01 × 10^2 0.61 × 10^2	This Work
	Deposition	PA, EF			10^3–10^8	3.97 × 10^3 1.55 × 10^3	

(SA and EF) and gram-negative (EC and PA) bacterial strains. The results highlighted the EET kinetics of these exoelectrogenic bacteria through their ability to reduce Fe(III) to Fe(II) in the PB coordination polymer. Raman and XPS analysis validated that the bacterial electron shuttles reduced PB into PW during the metabolic growth process. The PB/SPCEs showed notable sensitivity in the bacteria detection, with ranges of 10^2–10^8 CFU/mL for EC and SA, and 10^3–10^8 CFU/mL for PA and EF, along with consistent limits of detection. Bacterial viability was assessed within 3 hrs using growth curves and control studies in both bacterial culture buffer and real-time blood samples compared to conventional CO_2-based systems. These findings confirmed that PB-based electrodes are robust and catalytically efficient, making them sensitive for detecting electroactive bacterial metabolites responsible for BSIs in clinical settings. Future research will explore the impact of redox-influencing factors on sensors in blood samples and work on developing reliable electrochemical fingerprints for pathogen identification. This effort aims to enhance early detection and prevent the onset of sepsis.

CRediT authorship contribution statement

Sriramprabha Ramasamy: Writing – review & editing, Writing – original draft, Visualization, Validation, Methodology, Investigation, Formal analysis, Data curation, Conceptualization. **Sekar Madhu:** Writing – review & editing, Formal analysis. **Jungil Choi:** Writing – review & editing, Supervision, Resources, Project administration, Investigation, Funding acquisition, Data curation, Conceptualization.

Declaration of competing interest

The authors declare that they have no known competing financial interests or personal relationships that could have appeared to influence the work reported in this paper.

Acknowledgments

This study was supported by the Korea Disease Control and Prevention Agency (2024-ER2206-00) and the new faculty research fund at Ajou University. The authors express appreciation to Mukkath Joseph Josline from the Department of Energy Systems Research and the Department of Materials Science and Engineering at Ajou University for assistance with the material characterizations.

Appendix A. Supplementary data

Supplementary data to this article can be found online at https://doi.org/10.1016/j.bioelechem.2025.108902.

Data availability

Data will be made available on request.

References

[1] R.M. Martinez, D.M. Wolk, Bloodstream Infections, Microbiol Spectr. 4 (2016), https://doi.org/10.1128/microbiolspec.DMIH2-0031-2016.
[2] K. Lisowska-Łysiak, R. Lauterbach, J. Międzobrodzki, M. Kosecka-Strojek, Epidemiology and pathogenesis of staphylococcus bloodstream infections in humans: A review, Pol. J. Microbiol. 70 (2021) 13–23, https://doi.org/10.33073/PJM-2021-005.
[3] V. Russotto, A. Cortegiani, G. Graziano, L. Saporito, S.M. Raineri, C. Mammina, A. Giarratano, Bloodstream infections in intensive care unit patients: Distribution and antibiotic resistance of bacteria, Infect. Drug Resist. 8 (2015) 287–296, https://doi.org/10.2147/IDR.S48810.
[4] B. Santella, V. Folliero, G.M. Pirofalo, E. Serretiello, C. Zannella, G. Moccia, E. Santoro, G. Sanna, O. Motta, F. De Caro, P. Pagliano, M. Capunzo, M. Galdiero, G. Boccia, G. Franci, Sepsis—A retrospective cohort study of bloodstream infections, Antibiotics 9 (2020) 1–11, https://doi.org/10.3390/antibiotics9120851.
[5] B. Lamy, M. Sundqvist, E.A. Idelevich, Bloodstream infections – Standard and progress in pathogen diagnostics, Clin. Microbiol. Infect. 26 (2020) 142–150, https://doi.org/10.1016/j.cmi.2019.11.017.
[6] N. Peker, N. Couto, B. Sinha, J.W. Rossen, Diagnosis of bloodstream infections from positive blood cultures and directly from blood samples: recent developments in molecular approaches, Clin. Microbiol. Infect. 24 (2018) 944–955, https://doi.org/10.1016/j.cmi.2018.05.007.
[7] S.P. Costa, C.M. Carvalho, Burden of bacterial bloodstream infections and recent advances for diagnosis, Pathog. Dis. 80 (2022) 1–13, https://doi.org/10.1093/femspd/ftac027.
[8] O. Simoska, K.J. Stevenson, Electrochemical sensors for rapid diagnosis of pathogens in real time, Analyst 144 (2019) 6461–6478, https://doi.org/10.1039/c9an01747j.
[9] L.M. Castle, D.A. Schuh, E.E. Reynolds, A.L. Furst, Electrochemical Sensors to Detect Bacterial Foodborne Pathogens, ACS Sens. 6 (2021) 1717–1730, https://doi.org/10.1021/acssensors.1c00481.

[10] E. Koçak, C. Ozkul, B. Bozal-Palabiyik, İ. Süslü, B. Uslu, Electrochemical biosensors for rapid diagnosis of bacterial infections: Design, targets and applications in clinical setting, Electroanalysis 35 (2023) 1–16, https://doi.org/10.1002/elan.202300106.
[11] S. Madhu, S. Ramasamy, P. Manickam, P. Nagamony, V. Chinnuswamy, TiO2 anchored carbon fibers as non-invasive electrochemical sensor platform for the cortisol detection, Mater. Lett. 308 (2022) 131238, https://doi.org/10.1016/j.matlet.2021.131238.
[12] P. Manickam, S. Madhu, R.E. Fernandez, C. Viswanathan, S. Bhansali, Fabric based wearable biosensor for continuous monitoring of steroids, ECS Trans. 77 (2017) 1841–1846, https://doi.org/10.1149/07711.1841ecst.
[13] M. Sekar, R. Sriramprabha, P.K. Sekhar, S. Bhansali, Review — Towards wearable sensor platforms for the electrochemical detection of cortisol, J. Electrochem. Soc. 167 (2020) 067508, https://doi.org/10.1149/1945-7111/ab7e24.
[14] S. Madhu, S. Ramasamy, J. Choi, Recent developments in electrochemical sensors for the detection of antibiotic-resistant bacteria, Pharmaceuticals 15 (2022) 1488, https://doi.org/10.3390/ph15121488.
[15] R. Sriramprabha, M. Sekar, R. Revathi, C. Viswanathan, J. Wilson, Fe2O3/polyaniline supramolecular nanocomposite: A receptor free sensor platform for the quantitative determination of serum creatinine, Anal. Chim. Acta 1137 (2020) 103–114, https://doi.org/10.1016/j.aca.2020.09.004.
[16] M. Divagar, R. Sriramprabha, S. Sornambikai, N. Ponpandian, C. Viswanathan, Surface Imprinted Ag Decorated MnO2 Thin Film Electrodes for the synergic electrochemical detection of bacterial pathogens, J. Electrochem. Soc. 166 (2019) G1–G9, https://doi.org/10.1149/2.0711902jes.
[17] V. Templier, T. Livache, S. Boisset, M. Maurin, S. Slimani, R. Mathey, Y. Roupioz, Biochips for direct detection and identification of bacteria in blood culture-like conditions, Sci. Rep. 7 (2017) 9457, https://doi.org/10.1038/s41598-017-10072-z.
[18] M. Ajam-Hosseini, F. Akhoondi, F. Parvini, H. Fahimi, Gram-negative bacterial sRNAs encapsulated in OMVs: an emerging class of therapeutic targets in diseases, Front. Cell. Infect. Microbiol. 13 (2023), https://doi.org/10.3389/fcimb.2023.1305510.
[19] B. Péter, E. Farkas, S. Kurunczi, Z. Szittner, S. Bősze, I. Szekacs, R. Horvath, J. J. Ramsden, Review of label-free monitoring of bacteria: From challenging practical applications to basic research perspectives, Biosensors (Basel) 12 (2022) 188, https://doi.org/10.3390/bios12040188.
[20] S. Kaushal, S.S. Nanda, S. Samal, D.K. Yi, Strategies for the Development of metallic-nanoparticle-based label-free biosensors and their biomedical applications, Chembiochem 21 (2020) 576–600, https://doi.org/10.1002/cbic.201900566.
[21] Z. Guo, C. Yang, 5 Microbial metabolism kinetics and interactions in bioelectrosynthesis System, Wiley-VCH Verlag GmbH & Co., German, 2020, pp. 307–312.
[22] X. Liu, L. Shi, J.D. Gu, Microbial electrocatalysis: Redox mediators responsible for extracellular electron transfer, Biotechnol. Adv. 36 (2018) 1815–1827, https://doi.org/10.1016/j.biotechadv.2018.07.001.
[23] Y. Xiao, Z. Zheng, H. Gang, J. Ulstrup, F. Zhao, J. Zhang, High-resolution electrochemistry of the extracellular electron transfer of Escherichia coli 1, (n.d.). doi: 10.1101/2020.11.05.369678.
[24] O. Braissant, M. Astasov-Frauenhoffer, T. Waltimo, G. Bonkat, A review of methods to determine viability, vitality, and metabolic rates in microbiology, Front. Microbiol. 11 (2020) 547458, https://doi.org/10.3389/fmicb.2020.547458.
[25] Y. Dong, J. Zan, H. Lin, Bioleaching of heavy metals from metal tailings utilizing bacteria and fungi: Mechanisms, strengthen measures, and development prospect, J. Environ. Manage. 344 (2023) 118511, https://doi.org/10.1016/j.jenvman.2023.118511.
[26] A. Vincy, Y. Gaikwad, H. Agarwal, N. Jain, R. Vankayala, A label-free and ultrasensitive prussian blue-based dipstick sensor for bacterial and biofilm detection, Langmuir 39 (2023) 14246–14255, https://doi.org/10.1021/acs.langmuir.3c01451.
[27] J. Cai, Y. Lin, X. Yu, Y. Yang, Y. Hu, L. Gao, H. Xiao, J. Du, H. Wang, X. Zhong, P. Sun, X. Liang, H. Zhou, H. Cai, Multifunctional AuAg-doping prussian blue-based MOF: enhanced colorimetric catalytic activities and amplified SERS signals for bacteria discrimination and detection, Sens Actuators B Chem 394 (2023) 134279, https://doi.org/10.1016/j.snb.2023.134279.
[28] Y. Xu, Y. Jiang, C. Li, Y. Chen, Y. Yang, Integration of an XGBoost model and EIS detection to determine the effect of low inhibitor concentrations on E. coli, J. Electroanal. Chem. 877 (2020) 114534, https://doi.org/10.1016/j.jelechem.2020.114534.
[29] L. Leite, V. Pais, J. Bessa, F. Cunha, C. Relvas, N. Ferreira, R. Fangueiro, Prussian blue sensor for bacteria detection in personal protection clothing, Polymers (basel) 15 (2023) 872, https://doi.org/10.3390/polym15040872.
[30] C. Psotta, V. Chaturvedi, J.F. Gonzalez-Martinez, J. Sotres, M. Falk, Portable prussian blue-based sensor for bacterial detection in urine, Sensors 23 (2023) 388, https://doi.org/10.3390/s23010388.
[31] A. Ferrer-Vilanova, Y. Alonso, J.J. Ezenarro, S. Santiago, X. Muñoz-Berbel, G. Guirado, Electrochromogenic detection of live bacteria using soluble and insoluble prussian blue, ACS Omega 6 (2021) 30989–30997, https://doi.org/10.1021/acsomega.1c03434.
[32] Y. Wang, H. Xu, J. Zhang, G. Li, Electrochemical sensors for clinic analysis, Sensors 8 (2008) 2043–2081, www.mdpi.org/sensors.
[33] T.C. Babin, T. Dedole, P. Bouvet, P.R. Marcoux, M. Gougis, P. Mailley, Electrochemical label-free pathogen identification for bloodstream infections diagnosis: Towards a machine learning based smart blood culture bottle, Sens Actuators B Chem. 387 (2023) 133748, https://doi.org/10.1016/j.snb.2023.133748.
[34] N.B. Li, J.H. Park, K. Park, S.J. Kwon, H. Shin, J. Kwak, Characterization and electrocatalytic properties of Prussian blue electrochemically deposited on nano-Au/PAMAM dendrimer-modified gold electrode, Biosens. Bioelectron. 23 (2008) 1519–1526, https://doi.org/10.1016/j.bios.2008.01.009.
[35] S. Madhu, S. Ramasamy, V. Magudeeswaran, P. Manickam, P. Nagamony, V. Chinnuswamy, SnO2 nanoflakes deposited carbon yarn-based electrochemical immunosensor towards cortisol measurement, J Nanostructure Chem. 13 (2022) 115–127, https://doi.org/10.1007/s40097-022-00486-1.
[36] S. Watanabe, Y. Inaba, M. Harigai, K. Takeshita, J. Onoe, The uptake characteristics of Prussian-blue nanoparticles for rare metal ions for recycling precious metals from nuclear and electronic wastes, Sci. Rep. 12 (2022) 5135, https://doi.org/10.1038/s41598-022-08838-1.
[37] V. Jassal, U. Shanker1, Synthesis, Characterization and Applications of Nano-structured Metal Hexacyanoferrates: A Review, J. Environ. Anal. Chem. 02 (2015) 2. doi: 10.4172/2380-2391.1000128.
[38] J.B. Martins, S. Husmann, A.G. da Veiga, A.J.G. Zarbin, M.L.M. Rocco, Probing the electronic structure of prussian blue and analog films by photoemission and electron energy loss spectroscopies, ChemPhysChem 25 (2024) e202300590, https://doi.org/10.1002/cphc.202300590.
[39] A.M. Nawar, A.A. Alzharani, Impedance spectroscopy and conduction mechanism analysis of bulk nanostructure Prussian blue pellets, Mater. Chem. Phys. 306 (2023) 128000, https://doi.org/10.1016/j.matchemphys.2023.128000.
[40] H. Niwa, T. Moriya, T. Shibata, Y. Fukuzumi, Y. Moritomo, In situ IR spectroscopy during oxidation process of cobalt Prussian blue analogues, Sci. Rep. 11 (2021) 4119, https://doi.org/10.1038/s41598-021-83699-8.
[41] G. Moretti, C. Gervais, Raman spectroscopy of the photosensitive pigment Prussian blue, J. Raman Spectrosc. 49 (2018) 1198–1204, https://doi.org/10.1002/jrs.5366.
[42] B.F. Baggio, C. Vicente, S. Pelegrini, C.C.P. Cid, I.S. Brandt, M.A. Tumelero, A. A. Pasa, Morphology and structure of electrodeposited prussian blue and prussian white thin films, Materials 12 (2019) 1103, https://doi.org/10.3390/ma12071103.
[43] M. Lakshmi Narayanan, K. Prabhu, N. Ponpandian, C. Viswanathan, Cu encrusted RF sputtered ZnO thin film based electrochemical immunosensor for highly sensitive detection of IL-6 in human blood serum, Microchem. J. 199 (2024) 110061, https://doi.org/10.1016/j.microc.2024.110061.
[44] B. Niu, W. Jiang, B. Jiang, M. Lv, S. Wang, W. Wang, Determining the depth of surface charging layer of single Prussian blue nanoparticles with pseudocapacitive behaviors, Nat. Commun. 13 (2022) 2316, https://doi.org/10.1038/s41467-022-30058-4.
[45] S. Madhu, A.J. Anthuuvan, S. Ramasamy, P. Manickam, S. Bhansali, P. Nagamony, V. Chinnuswamy, ZnO Nanorod Integrated Flexible Carbon Fibers for Sweat Cortisol Detection, ACS Appl. Electron. Mater. 2 (2020) 499–509, https://doi.org/10.1021/acsaelm.9b00730.
[46] O.N. Oktyabrskii, G.V. Smirnova, Redox potential changes in bacterial cultures under stress conditions, Microbiology 81 (2012) 131–142, https://doi.org/10.1134/S0026261712020099.
[47] H. Wei, X.Y. Yang, H.C. van der Mei, H.J. Busscher, X-ray photoelectron spectroscopy on microbial cell surfaces: a forgotten method for the characterization of microorganisms encapsulated with surface-engineered shells, Front. Chem. 9 (2021) 666159, https://doi.org/10.3389/fchem.2021.666159.
[48] E.V. Suprun, E.V. Karpova, S.P. Radko, A.A. Karyakin, Advanced electrochemical detection of amino acids and proteins through flow injection analysis and catalytic oxidation on Prussian Blue, Electrochim. Acta 331 (2020) 135289, https://doi.org/10.1016/j.electacta.2019.135289.
[49] Q. Shi, Y. Teng, Z. Hu, Y. Zhang, W. Liu, One-step electrodeposition of Tris (hydroxymethyl) aminomethane – prussian blue on screen-printed electrode for highly efficient detection of glycosylated hemoglobin, Electroanalysis 31 (2019) 512–517, https://doi.org/10.1002/elan.201800644.
[50] J. Gao, L. Jeffries, K.E. Mach, D.W. Craft, N.J. Thomas, V. Gau, J.C. Liao, P. K. Wong, A multiplex electrochemical biosensor for bloodstream infection diagnosis, SLAS Technol. 22 (2017) 466–474, https://doi.org/10.1177/2211068216651232.
[51] E.M.K. Kurundu Hewage, D. Spear, T.M. Umstead, S. Hu, M. Wang, P.K. Wong, Z. C. Chroneos, E.S. Halstead, N.J. Thomas, An electrochemical biosensor for rapid detection of pediatric bloodstream infections, SLAS Technol. 22 (2017) 616–625, https://doi.org/10.1177/2472630317727704.
[52] S. Panhwar, H. Ilhan, S.S. Hassan, A. Zengin, I.H. Boyacı, U. Tamer, Dual responsive disposable electrode for the enumeration of escherichia coli in whole blood, Electroanalysis 32 (2020) 2244–2252, https://doi.org/10.1002/elan.202060185.
[53] R. Das, M.K. Sharma, V.K. Rao, B.K. Bhattacharya, I. Garg, V. Venkatesh, S. Upadhyay, An electrochemical genosensor for Salmonella typhi on gold nanoparticles-mercaptosilane modified screen printed electrode, J. Biotechnol. 188 (2014) 9–16, https://doi.org/10.1016/j.jbiotec.2014.08.002.
[54] D. Patel, Y. Zhou, R.P. Ramasamy, A Bacteriophage-based electrochemical biosensor for detection of methicillin-resistant staphylococcus aureus, J. Electrochem. Soc. 168 (2021) 057523, https://doi.org/10.1149/1945-7111/abef85.
[55] S.M. Imani, E. Osman, F. Bakhshandeh, S. Qian, S. Sakib, M. MacDonald, M. Gaskin, I. Zhitomirsky, D. Yamamura, Y. Li, T.F. Didar, L. Soleymani, Liquid

NanoBiosensors Enable One-Pot electrochemical detection of bacteria in complex matrices, Adv. sci. 10 (2023) 2207223, https://doi.org/10.1002/advs.202207223.
[56] N. Kumaragurubaran, P. Arul, S.T. Huang, C.H. Huang, S. Bin Fang, Y.H. Lin, Nanocatalyst coupled with a latent-ratiometric electrochemical switch for label-free zero-tolerance rapid detection of live Salmonella in whole blood samples, Sens Actuators B Chem 381 (2023) 133428, https://doi.org/10.1016/j.snb.2023.133428.
[57] W.N. Suryapratiwi, V.I. Paat, S. Gaffar, Y.W. Hartati, DNA biosensor for detection of Salmonella typhi from blood sample of typhoid fever patient using gold electrode modified by self-assembled monolayers of thiols, AIP Conference Proceedings 1848 (2017) 030005, https://doi.org/10.1063/1.4983937.